Journal Name

ARTICLE TYPE

Cite this: DOI: 10.1039/xxxxxxxxxx

Barriometry — an enhanced database of accurate barrier heights for gas-phase reactions†

Bun Chan[a,*] and John M. Simmie[b]

Received Date
Accepted Date

DOI: 10.1039/xxxxxxxxxx

www.rsc.org/journalname

The kinetics of very many reactions are critically dependent upon the barrier heights for which accurate determinations can be difficult. From the perspective of attaining such quantities using computational quantum chemistry, it is important to appropriately validate routine and efficient methodologies such as density functional theory (DFT) procedures. In the present study, we embark on the journey of establishing diverse databases using a consistent high-level quantum chemistry procedure, against which new and existing methodologies can be assessed. Thus, we have used the composite protocol W3X-L to provide refined reference values for existing databases [e.g., Zhao *et al., J. Phys. Chem. A*, 2005, **109**, 5656] and additionally establish benchmark data that are of interest to atmospheric and combustion chemists. While our endeavor has just begun, assessment of various DFT methods with our existing results lend support to the use of MN15 as an adequate method for general kinetics applications. We also recommend the use of the less-costly W2X and WG composite protocols for obtaining adequately accurate reference thermochemical values for larger molecular systems.

1 Introduction

Accurate reaction energy barriers are essential for obtaining reliable rate of a chemical reaction for application in astrochemistry, atmospheric, combustion and heterogeneously-catalysed chemistries.[1] Given the exponential dependence of the rate constant on barrier height, even a modest difference of 4.2 kJ mol^{-1} (1 kcal mol^{-1}, i.e., so called "chemical accuracy") leads to a five-fold change in the value of the reaction rate at room temperature. In this regard, the development of computational quantum chemistry has already progressed to the point where such accuracy can be routinely achieved using high-level (but computationally demanding) methods for small systems.[2]

For larger species, it is unavoidable to use computationally more efficient (but generally less accurate) methods such as density functional theory (DFT) procedures. In order to assess the suitability of DFT methods, a reliable database is required against which new and existing computational methods can be tested. For processes related to real-world atmospheric and combustion chemistries, currently no such database exists although recent work has made some headway.[3–5] Databases with alternative focuses have been created, notably for pericyclic[6], heterocyclic cycloreversion[7] and proton-exchange[8] reactions.

Here we focus on gas-phase reactions and adopt as our starting point the atom-transfer databases HTBH38[3] and NHTBH38.[9] They have already been previously employed for the purpose of assessing DFT procedures, notably as part of a recent extensive benchmark study.[10] To these databases we add an expanded palette of reaction types with relevance to atmospheric and combustion chemistries, among which recent high-level calculations exist for some.[11]

While general compendiums such as HTBH38 and specifically focused databases may be more suitable for testing theoretical methods rather than as a guide to reactions of direct real-world relevance, the objective of *this work* is to encompass both areas. We will use high-level methods that have been demonstrated to be of chemical accuracy to obtain data in this collection, in order to fulfill the goal of providing benchmark data for assessing methods that are less accurate (but rapidly improving through continuous development by the computational quantum chemistry community).

2 Computational details

A composite model chemistry, namely W3X-L, is employed.[12] As per recommendation by the original formulation and a recent benchmark study,[13] it utilizes, unless otherwise noted, geometries and frequencies obtained either with B3-LYP/cc-pVTZ+d or the double-hybrid density-functional theory (DH-DFT) DSD-PBE-P86/aug′-cc-pVTZ+d method.[14] To determine zero-point-

[a] *Graduate School of Engineering, Nagasaki University, Bunkyo 1-14, Nagasaki 852-8521, Japan; Tel: +81-92-802-2647; E-mail: bun.chan@nagasaki-u.ac.jp*
[b] *School of Chemistry, National University of Ireland, Galway, Ireland H91 TK33.*
† Electronic Supplementary Information (ESI) available: Optimized structures in xyz format, W3X-L and W2X vibrationless energies, and zero-point-vibrational energies. See DOI: 10.1039/b000000x/

vibrational energy, thermal correction to enthalpy, and entropy, the vibrational frequencies were scaled, respectively, by 0.9886, 0.9926 and 0.9970 for B3-LYP,[12] and 0.9830, 0.9876, and 0.9923 for DSD-PBE-P86.[13] These calculations were carried out with GAUSSIAN program.[15]

Energy determinations are then carried out by combining conventional and explicitly correlated[16,17] coupled-cluster computations, e.g., CCSD(T) and CCSD(T)-F12b,[18] extrapolated to the CBS limit with aug′-cc-pV*n*Z basis sets up to aug′-cc-pVQZ. Core-valence correlation and scalar-relativistic calculations were obtained, effectively, at the CCSD(T)/cc-pCVTZ level using non-relativistic frozen-core and all-electron Douglas-Kroll-Hess approaches and a combination of MP2 and CCSD(T) energies. These computations were carried out with MOLPRO.[19] This summarises the "W2X" component of W3X-L method. To arrive at the full W3X-L energy, post-CCSD(T) effects up to CCSDT(Q) are included, which were computed using the multi-reference code MRCC.[20,21]

A detailed overview of the performance of these protocols and related methods can be found elsewhere,[2,22] here we simply note that these models have been extensively tested, particularly in the calculation of enthalpies of formation by an atomisation procedure, as regards their performance against the best database of such values, the Active Thermochemical Tables or ATcT.[23] In practice W2X may not generally represent a significant advance over alternative composite methods such as G4[24] due to the implicit incorporation of high-level correlation effects within the empirical correction scheme in the latter. In comparison, the more advanced W3X-L provides a general improvement over W2X and G4 and was able to highlight outliers in the database.[25] Unless otherwise noted, in the main text, barriers correspond to the difference in zero-point corrected energies between the reactant(s) and the transition state, and is tabulated as $E^{\ddagger}$.

3 Results and discussion

3.1 W3X-L benchmark values for ATBH76

First of all, we employ the W3X-L protocol to provide refined reference data for the widely used HTBH38[3] and NHTBH38[9] data sets. These sets comprise a total of 76 (38 hydrogen-atom transfer and 38 non-hydrogen-atom transfer) reactions for small systems for which the computation with high-level post-CCSD(T) methods are computationally viable. Importantly, the compendium consists of a reasonably diverse collection of four types of processes, namely hydrogen-atom transfer, heavy-atom transfer, nucleophilic substitution, and unimolecular and association reactions. Such a diversity provides a good platform for the assessment of more-approximate quantum chemistry methods such as DFT. In the present study, we will refer to the complete set of 76 reactions as the ATBH76 (atom-transfer barrier height) set. The W3X-L vibrationless forward and reverse barriers for the ATBH76 database are shown in Table 1. We also provide in the supporting information the W3X-L free-energy values, which are more relevant to comparison with actual kinetic data.

Table 1 also contains alternative benchmark-quality values where data are available. Specifically, this include the DBH24/08 subset[26] where barriers have previously been obtained with (up to) the extremely high-level W4 protocol,[27] which employs very large basis sets up to aug′-cc-pV6Z and contains post-CCSD(T) terms up to CCSDTQ5. We note that, within the DBH24/08 database, three reactions have W4 benchmark values. They are $H + N_2O \longrightarrow OH + N_2$, $H + N_2 \longrightarrow HN_2$ and $HCN \longrightarrow HNC$. In these cases, our W3X-L barriers agree fairly well with the higher-level W4 values. While the comparisons are few with limited W4 data, the results do further support the quality of the W3X-L protocol as a cost-effective means for obtaining accurate thermochemical quantities. We will in later sections use these and W3X-L benchmark values for other data sets to assess the performance of a range of representative DFT methods for thermochemical applications.

It is noteworthy that, for this set of reactions, the CCSD(T)-based W2X performs very well, with an MAD of just 0.7 kJ mol^{-1} from our W3X-L benchmark values (see Supplementary Information). The good agreement between W2X and W3X-L is indicative

Table 1 W3X-L forward and reverse barrier heights (0 K, kJ mol^{-1}) for the ATBH76 data set, previous alternative high-level values obtained elsewhere[a] are shown in parentheses

Reaction	$E_f^{\ddagger}$	$E_r^{\ddagger}$
Hydrogen-atom transfer		
$H + HCl \longrightarrow H_2 + Cl$	17.9	18.4
$OH + H_2 \longrightarrow H + H_2O$	24.1	85.1
$CH_3 + H_2 \longrightarrow H + CH_4$	56.5	56.6
$OH + CH_4 \longrightarrow CH_3 + H_2O$	19.8 (21.7)	80.6 (81.5)
$H + H_2 \longrightarrow H_2 + H$	37.6	37.6
$OH + NH_3 \longrightarrow H_2O + NH_2$	11.5	60.7
$HCl + CH_3 \longrightarrow Cl + CH_4$	10.3	10.9
$OH + C_2H_6 \longrightarrow H_2O + C_2H_5$	8.7	85.1
$F + H_2 \longrightarrow HF + H$	3.5	139.9
$O + CH_4 \longrightarrow OH + CH_3$	45.6	39.8
$H + PH_3 \longrightarrow PH_2 + H_2$	10.0	102.6
$H + HO \longrightarrow H_2 + O$	41.8 (41.5)	47.5 (47.4)
$H + H_2S \longrightarrow H_2 + HS$	12.8 (12.6)	66.5 (67.2)
$O + HCl \longrightarrow OH + Cl$	31.5	26.3
$NH_2 + CH_3 \longrightarrow CH_4 + NH$	38.0	84.1
$NH_2 + C_2H_5 \longrightarrow C_2H_6 + NH$	39.3	69.7
$C_2H_6 + NH_2 \longrightarrow NH_3 + C_2H_5$	43.6	70.8
$NH_2 + CH_4 \longrightarrow CH_3 + NH_3$	56.6	68.2
s-trans−*cis*−$C_5H_8 \longrightarrow$ *s-trans*−*cis*−C_5H_8	157.5	157.5
Heavy-atom transfer		
$H + N_2O \longrightarrow OH + N_2$	76.8 (75.8)	339.9 (341.6)
$H + FH \longrightarrow HF + H$	167.9	167.9
$H + ClH \longrightarrow HCl + H$	68.7 (71.3)	68.7 (71.3)
$H + FCH_3 \longrightarrow HF + CH_3$	124.5	235.8
$H + F_2 \longrightarrow HF + F$	22.3	434.3
$CH_3 + FCl \longrightarrow CH_3F + Cl$	36.1 (36.2)	235.7 (238.8)
Nucleophilic substitution		
$F^- + CH_3F \longrightarrow FCH_3 + F^-$	−3.5	−3.5
$F^- \cdots CH_3F \longrightarrow FCH_3 \cdots F^-$	53.9	53.9
$Cl^- + CH_3Cl \longrightarrow ClCH_3 + Cl^-$	8.9	8.9
$Cl^- \cdots CH_3Cl \longrightarrow ClCH_3 \cdots Cl^-$	53.6 (53.9)	53.6 (53.9)
$F^- + CH_3Cl \longrightarrow FCH_3 + Cl^-$	−52.1	79.3
$F^- \cdots CH_3Cl \longrightarrow FCH_3 \cdots Cl^-$	13.3 (13.9)	118.7 (118.3)
$OH^- + CH_3F \longrightarrow HOCH_3 + F^-$	−8.2 (−6.9)	67.3 (68.3)
$OH^- \cdots CH_3F \longrightarrow HOCH_3 \cdots F^-$	46.5	195.0
Unimolecular and association		
$H + N_2 \longrightarrow HN_2$	64.4 (64.0)	27.8 (26.7)
$H + CO \longrightarrow HCO$	15.2	76.2
$H + C_2H_4 \longrightarrow CH_3CH_2$	13.2 (12.4)	158.6 (157.7)
$CH_3 + C_2H_4 \longrightarrow CH_3CH_2CH_2$	35.9	126.5
$HCN \longrightarrow HNC$	186.6 (187.3)	124.7 (124.8)

[a] Vibrationaless barriers of ref 26 plus ZPVEs of this work.

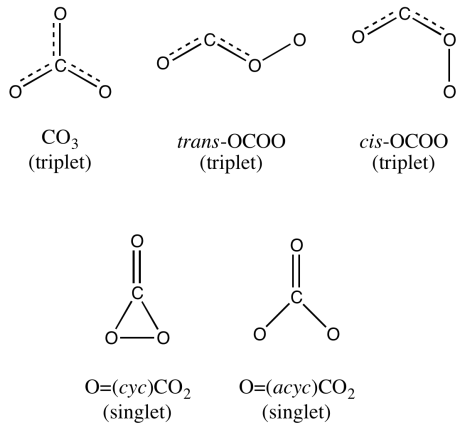

Fig. 1 Selected species examined on the "CO_3" potential-energy surface

of the predominantly-single-reference character of the species involved in the ATBH76 set. In passing, we also note that previously Curtiss *et al*.[28] had shown that G4 performs reasonably well against the selection of hydrogen-atom transfer reactions with a mean unsigned deviation of 3.8 kJ mol^{-1}. However, these generalised statistics do not tell the full story since for a key reaction $H + C_2H_4 \longrightarrow CH_3CH_2$ the error rises to ≈ 9 kJ mol^{-1}. They do show that the geometry underpinning G4, B3LYP/6-31G(2df,p), is partially responsible since using QCISD/MG3 geometries does reduce the deviations. As we shall see below, we also see the importance of utilizing highly accurate geometries, even in the context of already very high-level W*n*-type procedures.

3.2 "CO_3" and related reactions

A second set of reactions for which we have obtained refined reference values contains mainly species on the potential-energy surface of "CO_3". These include singlet and triplet trigonal CO_3 molecules of various geometries, *trans*- and *cis*- forms of (triplet) linearly connected O–C–O–O, and dissociated species CO_2 + $^3O/^1O$ and CO + $^3O_2$ (Fig. 1). These reactions are relevant from the perspective of areas such as atmospheric chemistry, interstellar chemistry, and bio-geo-chemistry. Our calculated forward and reverse barriers are shown in Table 2. Some of these are also the subject of a number of quantum chemistry investigations,[29–31] with a recent one undertaken using high-level methods up to W4.[31] In that study, three reactions were examined. They are $^3O + CO_2 \longrightarrow CO_3$, $^3O + CO_2 \longrightarrow$ *trans*–OCOO and $^3O + CO_2 \longrightarrow$ *cis*–OCOO.

In contrast to the good agreements between W3X-L and W4 for the ATBH76 set, for these "CO_3" reactions, the differences are larger. We find that this can be attributed to the use of different underlying geometries, namely DSD-PBE-P86 structures for W3X-L versus CCSD(T) for W4. The sensitivity of the geometries to the level of theory used to compute them highlights the difficulty in obtaining a reliable potential-energy surface (PES). We are currently in the process of conduction a thorough numerical construction of the PES using high-level methodologies, which will be the subject of a seperate publication. In the present study, for the sake of consistency for the comparison with additional CO_3 reactions, we retain the use of the double-hybrid-DFT geometries.

Table 2 Forward and reverse barrier heights for "CO_3" and related reactions (0 K, kJ mol^{-1}), previous alternative values obtained elsewhere[a] are shown in parentheses

Reaction	$E_f^{\ddagger}$	$E_r^{\ddagger}$
$^3O + CO_2 \longrightarrow CO_3$	90.2 (100.9)	5.8 (20.5)
$^3O + CO_2 \longrightarrow$ *trans*–OCOO	317.9 (313.4)	72.5
$^3O + CO_2 \longrightarrow$ *cis*–OCOO	259.0 (258.5)	11.3
trans–OCOO $\longrightarrow$ *cis*–OCOO	33.5	31.2
trans–OCOO $\longrightarrow$ CO + $^3O_2$	−6.3	204.1
cis–OCOO $\longrightarrow$ CO + $^3O_2$	−5.3	207.4
$^1O + CO_2 \longrightarrow O\cdots CO_2$	1.3 (energy of association)	
$^1O + CO_2 \longrightarrow O=(cyc)CO_2$	−93.5	115.2
$O=(cyc)CO_2 \longrightarrow O=(acyc)CO_2$	18.6	6.2
OH + $CO_2 \longrightarrow$ *trans*–OCOOH	309.4 (311.7)	24.9 (25.9)
trans–OCOOH $\longrightarrow$ CO + OOH	46.8 (47.7)	72.4 (74.9)

[a] Vibrationaless barriers from refs 31 and 32 plus ZPVEs of this work.

Our calculated barriers show that, on the triplet surface, the addition of ^3O to CO_2 would preferentially give trigonal CO_3 rather than linearly connected O–C–O–O by a substantial margin. This result is fully consistent with the conclusion drawn from previous W4 computations as well as from other studies mentioned above, and account for the production of O_2 being a minor outcome. The experimentally observed scrambling of oxygen atoms has previously been attributed to reactions on both the singlet and triplet surfaces by comparison with theoretical results. In particular, due to the high reactivity of ^1O, its addition to CO_2 proceeds with no forward barriers to form an CO_3 intermediate with a cyclic COO moiety. The low-barrier opening and re-closing of such three-membered rings then leads to the exchange of oxygen atoms. Alternatively, an addition/elimination route $^3O + CO_2 \longleftrightarrow CO_3$ is also viable. Our results in Table 2 are also consistent with such arguments.

In another study, the reactions OH + $CO_2 \longrightarrow$ *trans*–OCOOH and *trans*-OCOOH $\longrightarrow$ CO + OOH have been examined as part of a wider investigation.[32] These two reactions are relevant to the interconversion between, from one perspective, CO_2 and CO, and from another perspective OH and OOH. From the perspective of the "CO_3" reactions, they are analogous to the ^3O + $CO_2 \longrightarrow$ *trans*–OCOO and *trans*-OCOO $\longrightarrow$ CO + $^3O_2$ reactions, and show the "substituent" effect of a hydrogen atom in, e.g., OH versus ^3O. We can see that, while the additional hydrogen atom does not lead to a fundamental change in the reactivity for the $^3O + CO_2 \longrightarrow$ *trans*-OCOO reaction, the essentially irreversible *trans*-OCOO $\longrightarrow$ CO + $^3O_2$ reaction becomes close to thermal-neutral in the corresponding *trans*-OCOOH $\longrightarrow$ CO + OOH reaction.

3.3 Vinylperoxy radical reactions

A third set of reactions that we have examined are related to the vinylperoxy radical, which is a key intermediation in the reaction between the precursor vinyl radical and molecular oxygen. Notably, vinyl radical plays an important role in the combustion and pyrolysis of hydrocarbons. Its rich chemistry often dictates or play an important role in the outcome of related practical chemi-

Table 3 Forward and reverse barrier heights (0 K, kJ mol^{-1}) for reactions on the vinylperoxy radical potential energy surface, previous alternative values obtained elsewhere[a] are shown in parentheses

Reaction	$E_f^{\ddagger}$	$E_r^{\ddagger}$
W1 ⟶ W2	160.0 (157.7)	48.8 (47.3)
W1 ⟶ W3	95.2 (97.5)	52.0 (54.4)
W1 ⟶ W4	155.4 (149.0)	70.9 (64.4)
W3 ⟶ W5	−4.3	190.8
W4 ⟶ W6	5.4	281.9
W5 ⟶ W7	−1.8 (0.0)	116.9 (115.1)
W5 ⟶ W6	3.7 (7.5)	43.8 (43.9)
W7 ⟶ W8	165.2 (163.2)	166.1 (166.9)

[a] Alternative values from ref 11.

Table 4 Mean absolute deviations (kJ mol^{-1}) from benchmark W3X-L values for the ATBH76 set, the combined "CO_3" and "vinylperoxy radical" (ORBH36) set, and the complete set of all subsets for a wide-range of DFT methods and more-economical composite protocols

DFT	ATBH76	ORBH36	overall
B3-LYP and related methods			
B3-LYP	17.9	13.9	16.6
B3-PW91	15.9	14.6	15.5
BHandH-LYP	9.4	24.5	14.4
CAM-B3-LYP	11.8	14.2	12.6
PBE1-PBE and related methods			
PBE1-PBE	16.2	15.8	16.0
MPW1-PW91	14.1	14.8	14.3
TPSSh	26.5	18.2	23.8
LC-ωHPBE	7.3	17.2	10.5
HISSb-PBE	6.3	19.0	10.5
B98 and related methods			
B98	15.4	15.0	15.2
B1-B95	10.5	14.6	11.8
BMK	5.4	15.6	8.8
ωB97X	7.9	15.1	10.3
Minnesota functionals			
PW6-B95	12.6	14.7	13.3
M05	8.4	18.0	11.6
M05-2X	6.2	18.7	10.3
M06	8.7	15.9	11.1
M06-2X	5.2	19.6	9.9
M08-HX	4.1	20.4	9.4
MN15	5.6	14.9	8.6
M11	5.4	19.9	10.1
MN12-SX	4.7	16.3	8.5
Composite protocols			
WG	0.9	4.3	2.0
W2X	0.8	2.6	1.4

cal processes, which may at the one end be clean combustion but at the other end be dirty soot formation.[33]

In a recent study, Goldsmith *et al*. have investigated the reaction between vinyl radical and molecular oxygen using high-level quantum chemistry procedures.[11] The methodology that they employed is similar to W3X-L, in that it is a composite approach with CCSDT(Q) being the highest-level included. Specifically, their approach contains the term CCSDT(Q)/cc-pVDZ − CCSD(T)/cc-pVDZ. Thus, a difference from W3X-L in the post-CCSD(T) treatment is that the effect of CCSDT − CCSD(T) in the approach of ref 11 is not extrapolated, whereas such extrapolation is included in W3X-L. To this end, we have in the present study included a portion of the potential energy surface for vinylperoxy, $CH_2CHOO^{\bullet}$, with the aim to provide a cross validation of the values of ref 11, as well as to incorporate these reactions into our data set at a level that is consistent with the rest of reactions included here.

The reactions that we have examined here are those between the "wells" W1–W8 in ref 11. They represent sequential isomerization reactions of $CH_2CHOO^{\bullet}$ (W1). This set of reactions are depicted schematically in Fig. 2, and the reaction barriers are shown in Table 3. Our results are in reasonable agreements with those reported previously, though in some cases (e.g., $W_1 \longrightarrow W_4$) the discrepancies are more significant (but not excessive). We stress that the protocol employed by Goldsmith *et al*. are at a comparable level to W3X-L. Thus, in cases where notable differences occur in the computed barriers, we do not suggest one or the other to be a definitive benchmark value. Such discrepancies do indicate mild difficulties in the theoretical treatment of the species involved, and even-higher-level methodologies might be required to resolve the matters. At any rate, the downhill processes to produce W6–8 as major low-energy species are fully consistent with the reaction profile of ref 11.

While we are satisfied that our W3X-L 0 K barriers presented in this and previous sections are generally of chemical accuracy. For real-world kinetic applications, particularly those involved in high-energy processes, temperature-related factors are equally important, as elegantly demonstrated by Goldsmith *et al*. in ref 11. Such effects might not be fully captured by the simple protocol for geometry optimization and harmonic vibrational frequency calculations defined within W3X-L. At present, proper treatments of temperature effects remain complex and *ad hoc*, and the development of an accurate and "blackbox" approach is highly desirable in order to facilitate widespread use of highly accurate computational quantum chemistry for truly *in silico* kinetic studies.

3.4 Assessment of DFT procedures and lower-cost benchmark-quality composite protocols

An important use of compiling a set of highly accurate reaction barriers, further to their obvious practical applications in understanding real-world chemical phenomena, is to provide a benchmark for assessing more approximate methods. To this end, we note that the HTBH38 and NHTBH38 databases (i.e., ATBH76 set as referred to in the present study) have already been used extensively for such a purpose. It is of interest to see if the use of refined benchmark values provided by the present study will alter the conclusions drawn from previous works. Moreover, the provision of additional data for the "CO_3" and "vinylperoxy radical" sets will serve the purpose as an independent and, as we shall see, more challenging tests for the DFT methods. In the present study, we will refer to the combined "CO_3" and "vinylperoxy radical" sets as the ORBH36 set ("oxygen" reaction barrier heights).

A recent comprehensive benchmark study of an extensive set of DFT methods has confirmed the good overall performance of several Minnesota functionals.[10] In relation to the present study, the M06-2X and MN15 procedures have been shown in that work to be among the best performing methods for the HTBH38 and the NHTBH38 sets (i.e., the ATBH76 set). With our refined W3X-

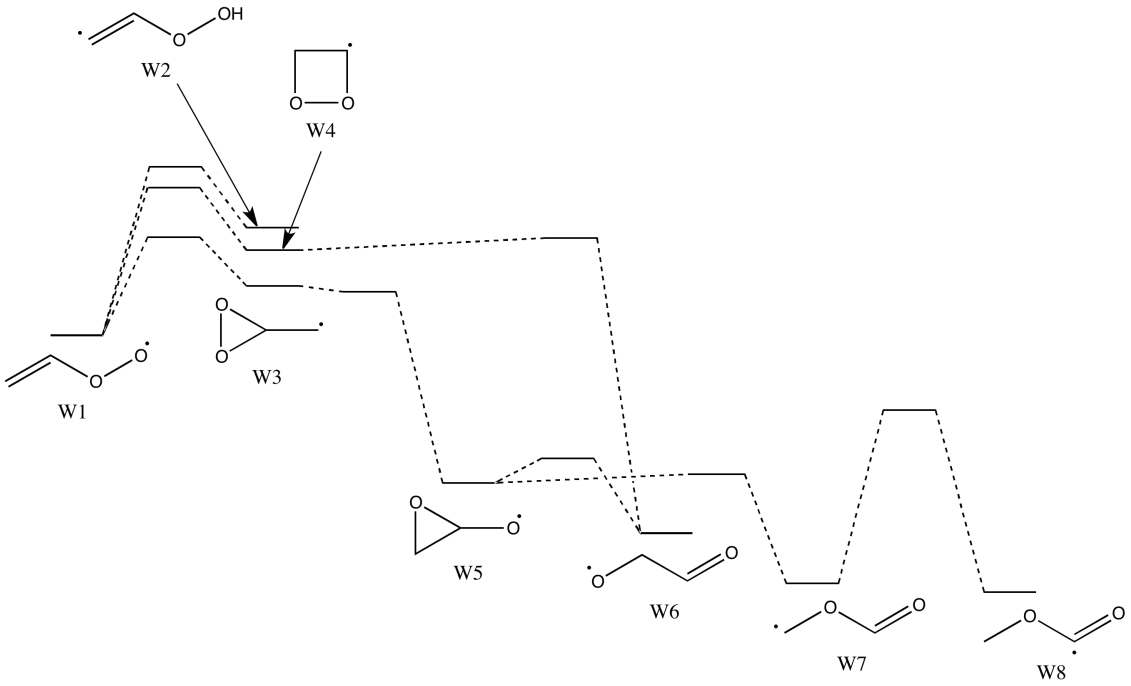

Fig. 2 Schematic reaction profile depicting "wells" (W) for some of the reactions in sequential isomerization of vinylperoxy radical ($CH_2CHOO^{\bullet}$, W1)

L benchmark values, we also find this to be the case. In addition, nearly all Minnesota functionals have fairly small mean absolute deviations (MADs) for the ATBH76 set. This is not surprising because these methods are typically parameterized with ATBH76 as one of the training sets. Other DFT methods that also give small MADs include for example the BMK and HISSb-PBE functionals.

The picture is rather different when one looks at the MADs for the ORBH36 set, for which none of the DFT procedures examined yields an MAD that is less than 15 kJ mol^{-1}. Interestingly, many of the older generation of functionals such as B3-LYP and MPW1-PW91 turn out to be better performers. At the other end of the spectrum, BHandH-LYP yields the largest MAD of 27.1 kJ mol^{1}. This finding appears to suggest that a large proportion of Hartree–Fock exchange is a contributing factor to large deviations for this set. With that being said, we note that the BMK and MN15 functionals have reasonable MAD values while also include reasonably large amount of Hartree–Fock exchange in their formulations. As we shall see below, the large deviations for BHandH-LYP is not a "Hartree–Fock problem" *per se*, but has more to do with the single-reference nature of common DFT methods (and Hartree–Fock). Overall, when one takes into account the results for both the ATBH76 and the ORBH36 sets, with a somewhat larger emphasis on the latter due to its more challenging nature, we consider MN15 to be the best performer in this assessment.

An important feature of DFT is its low cost and hence the capability for the computation of large molecular systems. Thus, while the identification of a best-performing DFT method for small species is significant, it is also important to assess their accuracy for calculating larger molecules. To this end, one would inevitably turning to lower-cost yet adequately accurate methods for obtaining benchmark quantities. We have therefore assessed the WG[22] and W2X[12] methods, in order to gauge the highest level of accuracy that one can reasonably expected when treating medium-sized molecules. These two methods are among the computationally efficient yet highly accurate W*n*X series of composite protocols.[12,22,34,35] While WG represents the most economical member within this family and is capable of treating molecules as large as coronene, W2X is the most accurate (for non-multi-reference systems) apart from W3X-L itself. We can see that, both methods are associated with MADs below 1 kJ mol^{-1} for the ATBH76 set. However, they are set apart by the more challenging ORBH36 set, for which the MADs are 2.6 and 4.3 kJ mol^{-1}, respectively, for W2X and WG. In any case, we believe these two methods are capable of providing benchmark-quality thermochemical quantities except for highly pathological cases.

3.5 Large deviations in the ORBH36 set

Detailed inspection of the individual deviations shows that the large MADs for ORBH36 are dominated by several exceedingly large deviations. The deviations for some of these for B3-LYP and BHandH-LYP are shown in Table 5. The choice of these two methods serves two purposes. First of all, as mentioned above, B3-LYP has one of the smallest MADs, while BHandH-LYP has the largest. Thus, they represent methods with performances at the two ends of the spectrum. Second, and perhaps more importantly, they share the same fundamental in their formulations, in that both are based on the B-LYP functional. The B3-LYP functional has 20% Hartree–Fock exchange, whereas BHandH-LYP has 50%. A comparison between the two thus enables us to gain some insights into the effect of varying the amount of Hartree–Fock exchange on the deviations from W3X-L benchmark values for these reactions.

An immediate observation from Table 5 is that, while the devi-

Table 5 Deviations (D, kJ mol^{-1}) from benchmark W3X-L values for selected reactions in the ORBH36 set for which the deviations for either the B3-LYP or the BHandH-LYP method are larger than 30 kJ mol^{-1}

Reaction	$D(E_f^{\ddagger})$	$D(E_r^{\ddagger})$
B3-LYP		
$^3O + CO_2 \longrightarrow$ *trans*−OCOO	−30.3	−8.1
$^1O + CO_2 \longrightarrow O=(cyc)CO_2$	8.7	60.8
$O=(cyc)CO_2 \longrightarrow O=(acyc)CO_2$	32.1	−14.2
$OH + CO_2 \longrightarrow$ *trans*−OCOOH	−16.3	−14.6
W1 $\longrightarrow$ W4	−55.6	−69.4
W4 $\longrightarrow$ W6	−0.5	24.3
BHandH-LYP		
$^3O + CO_2 \longrightarrow$ *trans*−OCOO	31.0	3.9
$^1O + CO_2 \longrightarrow O=(cyc)CO_2$	127.8	119.0
$O=(cyc)CO_2 \longrightarrow O=(acyc)CO_2$	81.4	−49.2
$OH + CO_2 \longrightarrow$ *trans*−OCOOH	37.0	6.2
W1 $\longrightarrow$ W4	−45.0	−58.8
W4 $\longrightarrow$ W6	14.8	59.9

ations for B3-LYP spread quite evenly between positive and negative values, most of the deviations for BHandH-LYP are positive. This is consistent with the general behavior of increasing barrier heights with the increasing proportion of Hartree–fock exchange. The many cases of large positive deviations is indicative of large correlation effects in the transition structure that are not sufficiently captured by the correlation functional. This is perhaps not surprising given that we would anticipate large multi-reference characters in the transition structures for some of these reactions. Among the six reactions considered, the one with the largest deviations is $^1O + CO_2 \longrightarrow O=(cyc)CO_2$ for which the BHandH-LYP barriers deviate from the benchmark W3X-L values by more than 100 kJ mol^{-1}. For this reaction, the deviations for B3-LYP in the forward direction is just 8.7 kJ mol^{-1} but the correspoinding value in the reverse direction is quite substantial (60.8 kJ mol^{-1}).

Let us now consider the transition structure of this reaction (Figure 3a). This "CO_3" species is a closed-shell singlet but one can intuitively expect a substantial open-shell character as the O–O bond in product, i.e., $O=(cyc)CO_2$ (b), is far from being fully formed. Indeed, the unrestricted B3-LYP and BHandH-LYP solutions for this transition structure have $\langle S^2 \rangle$ values of 0.94 and 0.99, respectively, which are substantially larger than the expectation value of zero for a pure singlet. When the UB3-LYP energy for the transition structure is used, the deviations for the forward and reverse barriers become −59.1 and −7.0 kJ mol^{-1}, respectively. For BHandH-LYP, the corresponding values are −2.7 and −11.6 kJ mol^{-1}. It has been suggested that unrestricted formulation is capable of partially capturing multi-reference characters such as those in stretched single bonds.[36] The vastly improved B3-LYP and BHandH-LYP barriers are consistent with such an argument.

3.6 Miscellaneous

The ATBH76 and ORBH36 sets discussed in previous sections represent reaction barrier data that are rather "self-contained". We are currently in the process of exploring a wider-range of systems to enrich the compendium for benchmark and kinetics purposes. In this section, we provide a glimpse of our investigations that have been undertaken. A number of mainly hydrogen-atom

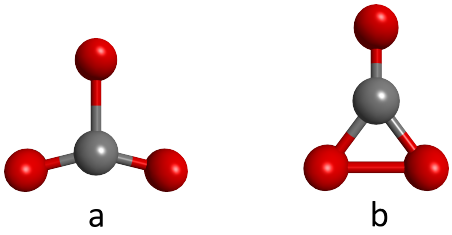

Fig. 3 Singlet transition structure (a) and product (b) for $^1O + CO_2 \longrightarrow O=(cyc)CO_2$

transfer reactions is presented in Table 6. Whereas in previous sections we provide our results in the form of forward and reverse barriers, here we show them as forward reaction barriers and reaction energies in order to enable a more direct comparison with literature values, including reaction energies evaluated from the tabulated enthalpies of formation in the Active Thermochemical Tables (ATcT).[23]. We note that in all cases the agreement is eminently satisfactory, and some specific cases will be discussed below.

H-atom abstraction from methane by both H-atom and hydroperoxyl radical are in very good agreement with the recent literature. An interesting observation is the comparison with the CCSD-R12//B3LYP/def2-TZVP result for $CH_4 + HO_2^{\bullet} \longrightarrow CH_3^{\bullet} + H_2O_2$,[38] which seems to suggest that this reaction does not involve very-high-level correlation effects. In the addition reaction, $H^{\bullet} + C_2H_4$, there is reasonable agreement with the QCISD(T)/CBS//QCISD(T)/cc-pVTZ work of Miller and Klippenstein.[40] Hydroperoxyl radical abstraction of an allylic hydrogen from propene is similarly in concordance with a zero-point corrected electronic energy barrier computed at the QCISD(T)/CBS//B3LYP/6-311++G(d,p) level.[39]

Swann *etal*. have recently carried out quantum Monte Carlo methods on H-abstraction by a hydrogen atom from methanol.[45] They also usefully summarise previous work on these reactions:

$$CH_3OH + H^{\bullet} \xrightarrow{TS1} {}^{\bullet}CH_2OH + H_2$$

$$CH_3OH + H^{\bullet} \xrightarrow{TS2} CH_3O^{\bullet} + H_2$$

We combine their vibrationless CCSD(T) barriers with our ZPVE values and find satisfactory agreement with our W3X-L barriers. A more detailed discussion of the consequences of these reactions has been addressed recently by Döntgen and Leonhard.[46] Similar abstractions by the hydroperoxy radical $HO_2^{\bullet}$ from methanol, studied by Klippenstein *etal*.[41] with CCSD(T)/CBS//CASPT2/cc-pVTZ, have $E_{1f}^{\ddagger}$ of 63.9 as against our W3X-L value of 64.0 kJ mol^{-1}. But the agreement is not as good for $E_{2f}^{\ddagger}$ where the W3X-L barrier is of 83.4 kJ mol^{-1}. It however agrees with the W2X value of 88.4 kJ mol^{-1}, and the significant post-CCSD(T) contribution is a clear indication that the multi-reference aspect is important. Our computed reaction energy at 0 K of 73.9 kJ mol^{-1} compares very favourably with an ATcT[23] derived value of 74.10 ± 0.41 kJ mol^{-1} (Table 6).

Shayan and Vahedpour have explored the reaction between methanol and ozone on a singlet potential energy surface at the

Table 6 Forward barrier heights ($E_f^{\ddagger}$) and reaction energies (ΔE_f) (kJ mol^{-1}) for an additional set of miscellaneous reactions

Reaction	$E_f^{\ddagger}$		ΔE_f	
	W3X-L	Lit.	W3X-L	Lit.[23]
$CH_4 + H \longrightarrow CH_3 + H_2$	57.0	54.3[37]	0.47	0.30 ± 0.10
$CH_4 + HO_2 \longrightarrow CH_3 + H_2O_2$	101.1	100.1[38]	72.4	71.71 ± 0.20
$CH_2CHCH_3 + HO_2 \longrightarrow CH_2CHCH_2 + H_2O_2$	66.4[a]	66.9[39]	2.2	-0.07 ± 0.61
$C_2H_4 + H \longrightarrow C_2H_5$	8.7	11.8[40]	−145.2	-146.07 ± 0.31
$CH_3OH + H \longrightarrow CH_2OH + H_2$	34.5	34.3[b]	−35.0	-36.45 ± 0.37
$CH_3OH + H \longrightarrow CH_3O + H_2$	55.1	55.3[b]	2.0	2.7 ± 0.38
$CH_3OH + HO_2 \longrightarrow CH_2OH + H_2O_2$	64.0	63.9[41]	36.9	34.95 ± 0.41
$CH_3OH + HO_2 \longrightarrow CH_3O + H_2O_2$	83.4	88.9[41]	73.9	74.10 ± 0.41
$CH_3OH + O_3(^1A_1) \longrightarrow H_2CO + trans\text{-}H_2O_3$	73.6	91.0[42]	−143.3	-141.35 ± 0.73
$CH_2O + O_3(^1A_1) \longrightarrow HCO + OOOH$	71.0	67.8[43], 72.2[44]	29.4	27.69 ± 0.19
$CH_2O + O_3(^1A_1) \longrightarrow cyclo\text{-}H_2(COOOO)$	69.7	79.9[43], 95.2[44]		48.5[43]

[a] W2X value. [b] Estimated from vibrationaless CCSD(T)/aug-cc-pVQZ value from ref 45 plus ZPVEs from *this work*.

[CCSD(T)//MP2]/6-311++G(d,p) level.[42] The PES is quite complex with a pre-reaction complex, intermediates and products including CH_2O, *cis* and *trans* dihydrogen trioxide or trioxidane, H_2O_3, and methanediol, $CH_2(OH)_2$. However what is of particular interest here is that the barrier heights which lead eventually to CH_2O + *cis*-H_2O_3 and to CH_2O + *trans*-H_2O_3 of 123 and 141 kJ mol^{-1} at MP2 level are completely reversed at CCSD(T) to 183 and 91 kJ mol^{-1}, respectively. This signifies the sensitivity of the results to the level of theory not just in absolute but also in relative terms. A look at Table 6 of the latter reaction shows significant difference between the literature CCSD(T) barrier and our W3X-L value. The corresponding W2X value of 78.2 kJ mol^{-1} indicates a significant basis set effect beyond 6-311++G(d,p) as well as a notable post-CCSD(T) contribution.

The H-abstraction reactions of singlet ground state ozone have not received much attention[47] but Voukides et al.[43] studied the radical abstraction of the acyl hydrogen in methanal and the addition across the double bond. Their results, which were obtained with [CCSD(T)//M05-2X]/6-311+G(d,p), show that the first process faces a barrier of 67.8 kJ mol^{-1} and the second a barrier of 79.9 kJ mol^{-1}. Wang *et al*. reported alternative barriers of 72.2 and 95.2 kJ mol^{-1}, respectively, calculated at the [BMC-CCSD//BHandH-YLP]/6-311+G(d,p) level.[44] Our results (Table 6) show that these barriers are in fact very similar; note that previously reported value of 68.4 (W3X-L) kJ mol^{-1} for $CH_2O + O_3(^1A_1) = HCO + OOOH$ were obtained with MN12-SX/6-311++G(d,p) geometries and frequencies,[47] which indicates a slight sensitivity to the underlying geometries.

Finally and briefly, both the singlet and triplet potential energy surfaces for the reactions of ketenyl radical ($HC{\equiv}C{-}O^{\bullet}$) with hydroxyl radical have been investigated by the Lin group.[48] Their CBS-QB3 results for $IM_7 \longrightarrow IM_8 \longrightarrow CH_2 + CO_2$ *via* TS15 and TS16, respectively, are shown in Fig. 4. These values are in good agreement with our W3X-L barriers of 153.4 and 46.3 kJ mol^{-1}, respectively. We also find good agreements for reaction energies.

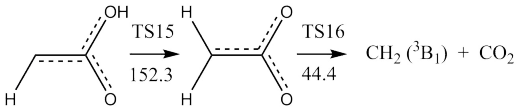

Fig. 4 A portion of the triplet potential energy surface for the reaction between ketenyl and hydroxy radicals

3.7 Uncertainties related to the use of DSD-PBE-P86 vibrational frequencies

So far our discussion focuses on the aspect of electronic energy. As mentioned previously,[12,13] within highly accurate composite protocols such as W3X-L, the use of thermochemical quantities [ZPVE, thermal correction to enthalpy (ΔH_{T-0}), and entropy (S_T)] calculated with DFT or DH-DFT vibrational frequencies may contribute significantly to the overall uncertainties. This factor might have different level of importance at different temperatures, given that both ΔH_{T-0} and S_T varies with the temperature. While ref 13 has given statistics for these quantities for stable species at 298 K, the uncertainties at other temperatures and those associated with calculated transition structures remain unclear. Among these two factors, it is straightforward to evaluate the uncertainties for stable species at different temperatures given the existing data provided by ref 13, and we will briefly explore this issue in the present study.

The LF10 set of benchmark thermochemical quantities have been used to assess the accuracy of using scaled DSD-PBE-P86/aug′-cc-pVTZ+d harmonic frequencies for their calculations.[13] This data set contains ten medium-sized molecules (PhH, PhF, PhCl, PhCN, cubane, CF_3CN, C_2F_6, N_2O_4, PF_5 and SF_6) with a total of 234 vibrational modes. In the present study, we have determined appropriate scale factors for ΔH_{T-0} and S_T at 500 and 1000 K according to the procedure given in ref 13. These scale factors, and the MADs for total enthalpies (H_T) and free energies (G_T) at 298, 500 and 1000 K for the LF10 set, are shown in Table 7.

It can be seen that, for this set of systems (with an average molecular size of ∼10 atoms), the MADs for H_T and G_T remain small in this temperature range. While the MAD for G_{1000} appears to be larger than those for G_{298} and G_{500}, when one takes into account the temperature factor on reaction rate according to standard Eyring equation, the effect of this uncertainty actually seems to become smaller with increasing temperature. Conversely, the uncertainties associated with these quantities can be expected to become more significant at lower temperatures. Un-

Table 7 Frequency scale factors for DSD-PBE-P86/aug′-cc-pVTZ+d for ZPVE, ΔH_{T-0} and S_T at 298, 500 and 1000 K, and MADs (kJ mol^{-1}) for the LF10 set of thermochemical quantities [total enthalpy (H_T) and free energy (G_T)] at these temperatures

Quantity	298 K	500 K	1000 K
ZPVE	0.9830	0.9830	0.9830
ΔH_{T-0}	0.9876	0.9808	0.9747
S_T	0.9923	0.9865	0.9812
MAD(H_T)	1.0	1.0	0.9
MAD(G_T	0.9	1.0	1.5

der these circumstances, other factors such as tunneling should also be considered. With these being said, we note that the MAD values shown here are for thermochemical quantities in *absolute* terms. For reaction energies and barriers, cancellation of deviations would often lead to lower relative deviations.[49]

4 Conclusions

The present study embarks on the establishment of a database of reaction barrier heights of closer link to real world chemistries with room for future expansion. Its purpose is to provide a consistent set of high-level theoretical numbers against which new model chemistries can be tested and, just as importantly, a check list for kinetic simulations of interest to different chemistries. Thus, we have used W3X-L, a composite protocol with the inclusion of high-level electron correlation effects up to CCSDT(Q), to provide accurate and consistent values for the ATBH76 and ORBH36 sets of over 100 reaction barriers. They cover a wide range of prototypical atom transfer reactions (ATBH76) and reactions related to oxygen species (ORBH36) with real-world relevance.

Comparison in cases where alternative high-level theoretical or accurate experimental values are available generally supports the quality of our W3X-L values. It also in a few cases highlights some remaining challenges. These include finding a computationally affordable and reliable geometry optimizer given that current work has been performed with relatively low-level B3-LYP and DSD-PBE-P86 methods. This is important because many real-world chemistries, such as those involved in the ORBH36 set, often involves "tricky" molecular transformations for which significant high-level correlation effects are involved, and therefore low-level optimization methods may yield erroneous structures. We also note that a straightforward and robust alternative to explicit anharmonic treatment is desirable for the determination of ro-vibrational modes including the all-important imaginary frequency for tunnelling corrections.

We have used the two high-level benchmark sets to assess a wide range of density-functional-theory procedures. For the ATBH76 set, our results are consistent with previous works, and they lend further support to the good accuracies of the Minnesota functionals such as the widely used M06-2X method and the latest MN15 functional. In contrast, none of the DFT methods examined has truly risen to the challenge presented by the more problematic ORBH36 set. With that being said, we note that some of the "multi-reference" issues may be partially alleviated by the use of the unrestricted formalism. Taking the results of both test sets into account, we perceive MN15 to be a reasonable choice for general kinetics applications within the limitation of current generation of DFT methods. We also note that, for expanded benchmark studies with larger molecular systems, the W2X and WG composite protocols could provide a computationally economical yet adequately accurate means for obtaining reference thermochemical values.

Acknowledgements

JMS thanks the Irish Centre for High-End Computing, ICHEC, for the provision of resources `ngche041c`. BC acknowledges funding from Japan Society for the Promotion of Science (grant number `16H07074001`) and computer time from the RIKEN Advanced Center for Computing and Communication (projects `Q16266` and `Q17266`) and Institute for Molecular Science, Japan.

References

1 D. Migliorini, H. Chadwick, F. Nattino, A. Gutiérrez-González, E. Dombrowski, E. A. High, H. Guo, A. L. Utz, B. Jackson, R. D. Beck and G.-J. Kroes, *J. Phys. Chem. Letts.*, 0, **0**, 4177–4182.

2 B. Chan, *Pure Appl. Chem.*, 2017, **89**, 699–713.

3 Y. Zhao and D. G. Truhlar, *J. Phys. Chem. A*, 2005, **109**, 5656–5667.

4 J. Zheng, Y. Zhao and D. Truhlar, *J. Chem. Theory Comput.*, 2007, **3**, 569–582.

5 G. J. Kroes, *J. Phys. Chem. Letts.*, 2015, **6**, 4106–4114.

6 A. Karton and L. Goerigk, *J. Comput. Chem.*, 2015, **36**, 622–632.

7 L. J. Yu, F. Sarrami, R. J. O'Reilly and A. Karton, *Chem. Phys.*, 2015, **458**, 1–8.

8 A. Karton, R. J. O'Reilly, B. Chan and L. Radom, *J. Chem. Theory Comput.*, 2012, **8**, 3128–3136.

9 Y. Zhao, B. J. Lynch and D. G. Truhlar, *Phys. Chem. Chem. Phys.*, 2005, **7**, 43–52.

10 N. Mardirossian and M. Head-Gordon, *Mol. Phys.*, 2017, **115**, 2315–2372.

11 C. F. Goldsmith, L. B. Harding, Y. Georgievskii, J. A. Miller and S. J. Klippenstein, *J. Phys. Chem. A*, 2015, **119**, 7766–7779.

12 B. Chan and L. Radom, *J. Chem. Theory Comput.*, 2015, **11**, 2109–2119.

13 B. Chan and L. Radom, *J. Chem. Theory Comput.*, 2016, **12**, 3774–3780.

14 S. Kozuch and J. M. L. Martin, *Phys. Chem. Chem. Phys.*, 2011, **13**, 20104–20107.

15 M. J. Frisch, G. W. Trucks, H. B. Schlegel, G. E. Scuseria, M. A. Robb, J. R. Cheeseman, G. Scalmani, V. Barone, G. A. Petersson, H. Nakatsuji, X. Li, M. Caricato, A. V. Marenich, J. Bloino, B. G. Janesko, R. Gomperts, B. Mennucci, H. P. Hratchian, J. V. Ortiz, A. F. Izmaylov, J. L. Sonnenberg, D. Williams-Young, F. Ding, F. Lipparini, F. Egidi, J. Goings, B. Peng, A. Petrone, T. Henderson, D. Ranasinghe, V. G. Zakrzewski, J. Gao, N. Rega, G. Zheng, W. Liang, M. Hada, M. Ehara, K. Toyota, R. Fukuda, J. Hasegawa, M. Ishida, T. Nakajima, Y. Honda, O. Kitao, H. Nakai, T. Vreven, K. Throssell, J. A.

Montgomery, Jr., J. E. Peralta, F. Ogliaro, M. J. Bearpark, J. J. Heyd, E. N. Brothers, K. N. Kudin, V. N. Staroverov, T. A. Keith, R. Kobayashi, J. Normand, K. Raghavachari, A. P. Rendell, J. C. Burant, S. S. Iyengar, J. Tomasi, M. Cossi, J. M. Millam, M. Klene, C. Adamo, R. Cammi, J. W. Ochterski, R. L. Martin, K. Morokuma, O. Farkas, J. B. Foresman and D. J. Fox, *Gaussian-16 Revision A.03*, 2016, Gaussian Inc. Wallingford CT.

16 S. Ten-no and J. Noga, *WIREs Comput. Mol. Sci.*, 2012, **2**, 114–125.

17 A. GrÃijneis, S. Hirata, Y. ya Ohnishi and S. Ten-no, *J. Chem. Phys.*, 2017, **146**, 080901.

18 T. B. Adler, G. Knizia and H.-J. Werner, *J. Chem. Phys*, 2007, **127**, 221106.

19 H.-J. Werner, P. J. Knowles, G. Knizia, F. R. Manby, M. Schütz *et al.*, *MOLPRO, version 2010.1, a package of ab initio programs*, Cardiff, UK.

20 M. Kállay, Z. Rolik, J. Csontos, P. Nagy, D. M. G. Samu, I. Ladjánszki, L. Szegedy, B. Ladóczki, K. Petrov, M. Farkas and B. Hégely, *MRCC, a quantum chemical program suite*, 2013.

21 Z. Rolik, L. Szegedy, I. Ladjanszki, B. Ladoczki and M. Kállay, *J. Chem. Phys.*, 2013, **139**, 094105.

22 B. Chan, *J. Chem. Theory Comput.*, 2017, **13**, 2642–2649.

23 B. Ruscic and D. H. Bross, *Active Thermochemical Tables (ATcT) values based on ver. 1.122 of the Thermochemical Network*, 2016, available at ATcT.anl.gov, accessed 2017–09–15.

24 L. A. Curtiss, P. C. Redfern and K. Raghavachari, *J. Chem. Phys.*, 2007, **126**, 084108.

25 J. M. Simmie and J. N. Sheahan, *J. Phys. Chem. A*, 2016, **120**, 7370–7384.

26 J. Zheng, Y. Zhao and D. G. Truhlar, *J. Chem. Theory Comput.*, 2009, **5**, 808–821.

27 A. Karton, E. Rabinovich, J. M. L. Martin and B. Ruscic, *J. Chem. Phys.*, 2006, **125**, 144108.

28 L. A. Curtiss, P. C. Redfern and K. Raghavachari, *Chem. Phys. Letts.*, 2010, **499**, 168–172.

29 R. D. J. Froese and J. D. Goddard, *J. Phys. Chem.*, 1993, **97**, 7484–7490.

30 C. J. Bennett, C. Jamieson, A. M. Mebel and R. I. Kaiser, *Phys. Chem. Chem. Phys.*, 2004, **6**, 735–746.

31 L. Y. Yeung, M. Okumura, J. Zhang, T. K. Minton, J. T. Paci, A. Karton, J. M. L. Martin, J. P. Camden and G. C. Schatz, *J. Phys. Chem. A*, 2012, **116**, 64–84.

32 X. You, H. Wang, E. Goos, C.-J. Sung and S. J. Klippenstein, *J. Phys. Chem. A*, 2007, **111**, 4031–4042.

33 M. Frenklach, *Phys. Chem. Chem. Phys.*, 2002, **4**, 2028–2037.

34 B. Chan and L. Radom, *J. Chem. Theory Comput.*, 2012, **8**, 4259–4269.

35 B. Chan and L. Radom, *J. Chem. Theory Comput.*, 2013, **9**, 4769–4778.

36 J. W. Hollett and P. M. W. Gill, *J. Chem. Phys.*, 2011, **134**, 114111.

37 J. Li, J. Chen, Z. Q. Zhao, D. Q. Xie, D. H. Zhang and H. Guo, *J. Chem. Phys.*, 2015, **142**, 204302.

38 J. Aguilera-Iparraguirre, H. J. Curran, W. Klopper and J. M. Simmie, *J. Phys. Chem. A*, 2008, **112**, 7047–7054.

39 J. Zádor, S. J. Klippenstein and J. A. Miller, *J. Phys. Chem. A*, 2011, **115**, 10218–10225.

40 J. A. Miller and S. J. Klippenstein, *Phys. Chem. Chem. Phys.*, 2004, **6**, 1192–1202.

41 S. J. Klippenstein, L. B. Harding, M. J. Davis, A. S. Tomlin and R. T. Skodje, *Proc. Combust. Inst.*, 2011, **33**, 351–357.

42 K. Shayan and M. Vahedpour, *Prog. React. Kinet. Mech.*, 2014, **39**, 171–185.

43 A. C. Voukides, K. M. Konrad and R. P. Johnson, *J. Organic Chem.*, 2009, **74**, 2108–2113.

44 F. Wang, H. Sun, J. Y. Sun, X. J. Jia, Y. J. Zhang, Y. Z. Tang, X. M. Pan, Z. M. Su, L. Z. Hao and R. S. Wang, *J. Phys. Chem. A*, 2010, **114**, 3516–3522.

45 E. T. Swann, M. L. Coote, A. S. Barnard and M. C. Per, *Int. J. Quantum Chem.*, 2017, **117**, 25361.

46 M. DÃűntgen and K. Leonhard, *J. Phys. Chem. A*, 2017, **121**, 1563–1570.

47 J. Würmel and J. M. Simmie, *J. Phys. Chem. A*, 2017, **121**, 8053–8060.

48 T. V. T. Mai, P. Raghunath, X. T. Le, L. K. Huynh, P. C. Nam and M. C. Lin, *Chem. Phys. Lett.*, 2014, **592**, 175–181.

49 B. Chan, *J. Chem. Theory Comput.*, 2017, **13**, 6052–6060.

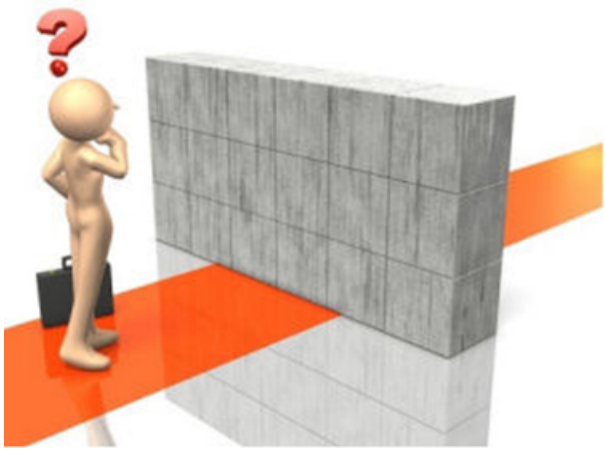

Fig. 5 TOC graphic